# Spin-State Dependent Properties of an Iron(III) Hydrogenase Mimic

**Eileen Edler[a] and Matthias Stein*[a]**

**Keywords:** mononuclear Fe(III) / proton reduction / spin transition / hydrogenases

A biomimetic mononuclear iron(III) model complex was investigated in detail using density functional theory (DFT) calculations. Structural and energetic criteria were employed to confirm the S=3/2 intermediate state to be the ground state. The ground state was verified using both pure and hybrid functionals with a different amount of exact Hartree Fock exchange. A comprehensive study of the influence of the functional as well as thermodynamic corrections on the energetic ordering of spin states was performed. A modified B3LYP functional with 10% of Hartree Fock exchange was able to reproduce the structural properties in excellent agreement with experimental data (A. Begum, S. Sarkar, Eur. J. Inorg. Chem., 2012, 10.1002/ejic.201100879). The thermodynamics of two possible spin crossover transitions (IS/HS), (LS/HS) were investigated. A torsional profile obtained by rotation of the axial ligand revealed a spin-dependent preference of the ligand orientation. The structure solved by X-ray crystallography corresponds to the global energetic minimum of the complex in the S=3/2 and S=5/2 state but not in the S=1/2 state. This study demonstrates that the spin multiplicity affects not only the structural properties but may also influence the chemical reactivity of this transition metal complex in general.

## Introduction

Using fossil fuels like coal, oil, and natural gas as today's major energy sources leads to carbon dioxide as a combustion product, an increase in global temperature and long-term climate changes. In the quest for alternative, sustainable fuels to satisfy the increasing world-wide demand for energy, hydrogen has been identified as a potential candidate for a "clean fuel", see for example.[1] For a recent review about hydrogen generation possibilities, storage, and usage see[2]. Enzymes from bacteria or archaea, termed 'hydrogenases', are able to convert electrons and protons to molecular hydrogen:[3]

$$H^+ + H^- \rightleftharpoons H_2$$

According to their active site compositions, they are distinguished as [NiFe]- and [FeFe]-hydrogenases as well as FeS cluster-free [Fe]-hydrogenases.[4] The first two classes are of interest to biological and chemical investigations due to their ability to serve as catalysts for electrochemical hydrogen production. In particular, [FeFe]-hydrogenases are of biotechnological relevance due to their high turnover numbers.[5] Structural details of [FeFe]-hydrogenase enzymes were elucidated by different spectroscopic techniques like X-ray protein crystallography[6] which provided valuable insight into the enzymatic catalytic functionality (for a review see[7]).

The [FeFe]-hydrogenase active site consists of a six-iron cluster, termed the 'H-cluster'. A cubane [4Fe-4S] cluster is connected to a dinuclear iron cluster via the sulphur ligand of a cysteine amino acid (see Figure 1A). The dinuclear FeFe cluster is the site of catalytic turnover: proton binding, reduction and hydrogen release. The cubane probably serves as an electron relay and shuttles electrons to the two other [4Fe-4S] cubane clusters. The iron atoms of the dinuclear site are labelled according their position to the H-cluster cubane as 'proximal' $Fe_p$ and 'distal' $Fe_d$. The distal iron atom shows an open coordination site and is the site of catalysis.[9] During the catalytic cycle, the FeFe cluster shuttles between different Fe-Fe oxidation states (i.e. mixed valence Fe(II)Fe(I) in the oxidized state and Fe(I)-Fe(I) in the reduced state).[10] The iron atoms are stabilized in their low-spin states by inorganic $CN^-$ and CO ligands causing a strong ligand field and connected by a dithiolate ligand which was recently assigned to be an azadithiolate (adt) ligand. [7], [11]

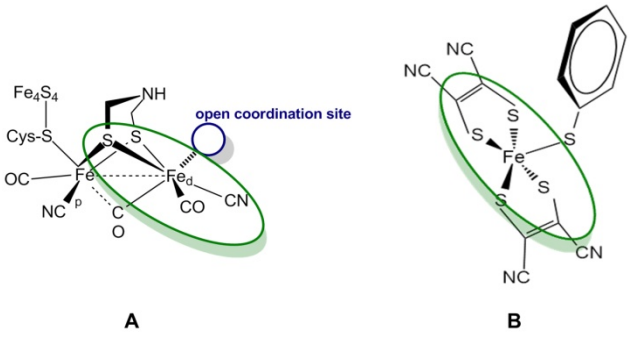


Figure 1. Schematic representation of the [FeFe]-hydrogenase active site (**A**) and complex **1**, a penta-coordinate Fe(III) functional mimic of hydrogenase [8] (**B**).

The active site assembly of [FeFe]-hydrogenases is a source and challenge for the design and synthesis of biomimetic model complexes. Today, more than 250 synthetic iron complexes were investigated that structurally and/or functionally mimic the active site of [FeFe]-hydrogenases (for reviews see[12],[13]). Since only the distal $Fe_d$ is the site of proton binding and reduction, mononuclear iron complexes were designed and investigated as functional

[a] Max-Planck-Institut for Dynamics of Complex Technical Systems, Molecular Simulations and Design Group, Sandtorstrasse 1, 39106 Magdeburg, Germany
E-mail: matthias.stein@mpi-magdeburg.mpg.de
Homepage: http://www.mpi-magdeburg.mpg.de
Supporting information for this article is available on the WWW under http://www.eurjic.org/ or from the author.

models for the [FeFe]-hydrogenase.[14] Mononuclear complexes containing iron(II)[15],[16] and iron(III)[8] have recently been synthesized and functionally studied. Kaur-Ghumaan *et al*.[15] showed that a mononuclear iron(II) complex is able to evolve molecular hydrogen involving two steps of proton reduction. A recently published penta-coordinate iron(III) dithiolene complex was shown to catalyse $H_2$ evolution at a mild overpotential of 0.3 V vs. Ag/AgCl.[8] This $[Fe^{III}\text{-}(mnt)_2(SPh)]^{2-}$ complex (Figure 1B, mnt = maleonitrile dithiolate, complex **1**) has a distorted square-pyramidal geometry. The iron forms an almost basal plane with four sulphur atoms of the maleonitrile dithiolate ligands. A thiophenolate ligand is axially coordinated to the iron atom. The chemistry of iron 1,2-dithiolates as redox non-innocent ligands has been investigated in detail (see review articles[17],[18] and in monographs[19]).

Iron(III) complexes can exist in different spin states, depending on the distribution of the 5 d-electrons in the iron 3d orbitals. In principle, complex **1** can adopt the low-spin doublet (S=1/2), the intermediate-spin quartet (S=3/2), or the high-spin (S=5/2) state (Figure 2). From EPR spectroscopy and magnetic susceptibility measurements, an electronic S=3/2 ground state was suggested for complex **1**.[8]

For open shell transition metal complexes, Kohn-Sham Density Functional Theory (DFT) provides results in good agreement with experiment in inorganic[20] and bioinorganic chemistry.[21] For example, Reiher showed that DFT is able to accurately describe transition metal complexes in terms of structural parameters. However, an adjustment of the admixture of exact Hartree-Fock (HF) exchange to 15% in the hybrid B3LYP functional was necessary to obtain a correct order of spin states.[22],[23]

Such a correct calculation of different spin state energies is particularly important when investigating spin crossover (SCO) compounds. These are characterised by a small energy difference between the ground spin state and a higher spin state with different multiplicity, such that an external stimulus can induce a change of spin state. There are many metal complexes, especially iron(II) complexes, described to undergo spin crossover but much less iron(III) complexes (for reviews on spin crossover phenomena see[24],[25]). Most characterised iron(III) spin crossover compounds undergo a transition from low-spin to high-spin states but less frequently from the intermediate-spin ground state (such as complex **1)** to another spin state.

The relative energetic ordering of the three possible spin states of complex **1** represents a benchmark. We aimed at a discrimination of the three possible spin states of complex **1** by DFT calculations. Structural and electronic properties of complex **1** were obtained for all three spin states and compared with experimentally found bond distances and angles. Structural parameters of complex **1** are sensitive to the spin state of the central iron(III) metal. In particular, the distance between the central iron atom and the axially bound thiophenolate ligand can be used as an indicator for the spin states. Our results confirm the experimentally determined S=3/2 spin state to be the electronic ground state of complex **1**. The relative energetic order of the low- and high-spin states, however, was found to be dependent on the amount of Hartree-Fock exchange in hybrid DFT calculations.
Calculations using a modified B3LYP functional with 10% HF exchange (B3LYP** [22],[23],[26]) gave excellent results. The ordering of the spin states of complex **1** is also found to be

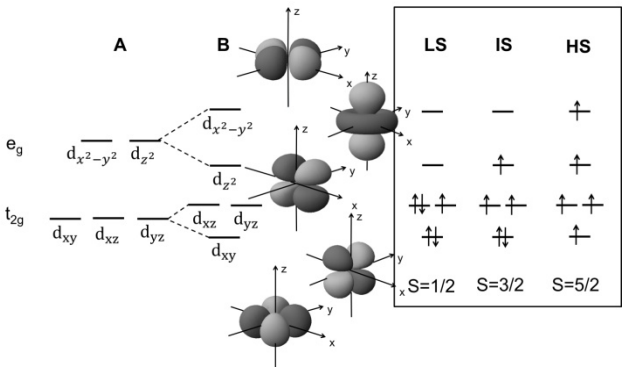


Figure 2. Crystal field splitting of the 3d orbitals in **A)** an octahedral system and **B)** a penta-coordinate square-pyramidal complex. For iron(III) the $3d^5$ electron occupancies are shown for the low-spin (LS) S=1/2 state, the intermediate-spin (IS) S=3/2 state, and the high-spin (HS) S=5/2 state.

temperature-dependent due to the different influence of entropic contributions to the spin states' Gibbs energies. Thus, complex **1** shows the behaviour of a spin crossover compound, usually observed for octahedrally-coordinated compounds[27] between low- and high-spin states.

In addition, a preferred spin state-dependent orientation of the axial ligand is observed and analysed in terms of orbital interactions. We show that the conformation of the X-ray structure corresponds to the global energetic optimum on the S=3/2 potential energy surface, whereas in the S=1/2 state the axial ligand prefers an almost perpendicular orientation.

## Results and Discussion

### Spin state-dependent structural parameters and ground state

The effect of the iron(III) spin state on the structural parameters of complex **1** (Figure 1B) and the relative energetic ordering of the S=1/2 (low-spin, LS) , S=3/2 (intermediate-spin, IS), and S=5/2 (high-spin, HS) states was investigated using the BP86 and B3LYP functionals. It was ensured that the S=1/2, S=3/2, and S=5/2 spin states are magnetically distinguishable pure spin states by analysis of the calculated $\langle \hat{S}^2 \rangle$ values (see Supplementary Information, Table S3). Depending on the functional, only minor deviations from the expectation value were observed, rendering quantum mechanical mixtures of spin states extremely unlikely. The calculated structural parameters for the S=1/2, S=3/2 and S=5/2 states of complex **1** are given in Table 1 (see below). In general, both the spin state and the choice of the functional appeared to be critical for the accuracy of the calculation of structural parameters. Overall RMSD values show that the experimental data are best reproduced by the BP86 functional (RMSD for S=3/2: 0.26 Å in BP86 vs. 0.30 Å in B3LYP calculations). In general, the BP86 functional shows a better agreement with the crystal structure regarding bond lengths compared to the B3LYP functional. For the S=3/2 state the deviation of the Fe-$S_{eq}$ bonds is only 0.01 Å with the BP86 functional compared to 0.04 Å with the B3LYP functional (Table 1 and Figure 3). Bond angles are equally well described with BP86 and B3LYP calculations. The B3LYP functional, on the other hand, gives dihedral angles in slightly better agreement with the X-ray structure than the BP86 functional.

Table 1. Relevant spin state-dependent structural parameters of complex **1**.

| Calculation | Structural parameters | X-ray structure[8] | Low Spin S=1/2 | Intermediate Spin S=3/2 | High Spin S=5/2 |
|---|---|---|---|---|---|
| BP86/ def2-TZVP | Distances | | | | |
| | Fe-$S_{eq}$ [a] | 2.27 Å | 2.22 Å | 2.26 Å | 2.42 Å |
| | Fe-$S_{ax}$ | 2.36 Å | 2.23 Å | 2.39 Å | 2.34 Å |
| | $S_1\cdots H_{10}$ | 3.14 Å | 2.99 Å | 2.97 Å | 3.11 Å |
| | $S_2\cdots H_{10}$ | 2.91 Å | 3.07 Å | 3.14 Å | 3.17 Å |
| | Angles | | | | |
| | <(S-Fe–S) [b] | 88.8° | 89.4° | 88.1° | 85.3° |
| | <(S-Fe-S) [c] | 85.6° | 88.7° | 87.5° | 89.0° |
| | <(Fe–plane) [d] | 152.4° | 159.4° | 155.6° | 146.3° |
| | <($S_{eq}$–$S_{ax}$) [e] | 103.7° | 100.2° | 102.1° | 106.5° |
| | <(Fe–$S_5$–$C_9$) | 113.7° | 116.7° | 117.8° | 116.0° |
| | Torsional Angles | | | | |
| | <($S_1$–Fe–$S_5$–$C_9$) | 66.8° | 64.3° | 53.7° | 52.0° |
| | <($S_2$–Fe–$S_5$–$C_9$) | 0.0° | -0.3° | -10.6° | -11.0° |
| | <(Fe–$S_5$–$C_9$–$C_{10}$) | 336.2° | 323.4° | 338.5° | 336.6° |
| | RMSD [f] | - | 0.34 Å | 0.26 Å | 0.38 Å |
| B3LYP/ def2-TZVP | Distances | | | | |
| | Fe-$S_{eq}$ [a] | 2.27 Å | 2.28 Å | 2.31 Å | 2.44 Å |
| | Fe-$S_{ax}$ | 2.36 Å | 2.29 Å | 2.44 Å | 2.37 Å |
| | $S_1\cdots H_{10}$ | 3.14 Å | 3.01 Å | 3.03 Å | 3.10 Å |
| | $S_2\cdots H_{10}$ | 2.91 Å | 3.28 Å | 3.30 Å | 3.34 Å |
| | Angles | | | | |
| | <(S-Fe-S) [b] | 88. 8° | 88.4° | 87.5° | 85.1° |
| | <(S-Fe-S) [c] | 85. 6° | 88.6° | 87.9° | 89.3° |
| | <(Fe–plane) [d] | 152.4° | 157.3° | 154.8° | 147.5° |
| | <($S_{eq}$–$S_{ax}$) [e] | 103.7° | 101.2° | 102.6° | 106.2° |
| | <(Fe–$S_5$–$C_9$) | 113.7° | 114.2° | 116.6° | 114.8° |
| | Torsional Angles | | | | |
| | <($S_1$–Fe–$S_5$–$C_9$) | 66.8° | 66.4° | 56.6° | 54.1° |
| | <($S_2$–Fe–$S_5$–$C_9$) | 0.0° | +1.7° | -7.0° | -8.0° |
| | <(Fe–$S_5$–$C_9$–$C_{10}$) | 336.2° | 316.7° | 329.8° | 327.3° |
| | RMSD [f] | - | 0.39 Å | 0.30 Å | 0.38 Å |

[a] Averaged over all equatorial Fe-S bonds. [b] Averaged over the bond angles S-Fe-S of each mnt ligand. [c] Averaged over the bond angles S-Fe-S of opposite mnt ligands. [d] Averaged over the bond angles S-Fe-S forming the plane. [e] Averaged over the bond angles each $S_{eq}$-Fe-$S_{ax}$. [f] The root mean square deviation (RMSD) was calculated from the superposition of X-ray and optimized structures (Figure 3).

The torsion angle θ, the angle that describes the orientation of the axial $SPh^-$ ligand (see Figure 8), differs from experiment by 11° for the BP86 functional but only by 7° for the B3LYP functional in the S=3/2 state structure. Independent from the functional, the central metal atom's spin multiplicity strongly influences the structural parameters. Optimized structural parameters in the high-spin state differ more from those obtained in the crystal structure. The RMSD value for the S=5/2 state is 0.38 Å for both, the BP86 and the B3LYP functionals. In particular, the equatorial metal-ligand bond lengths are substantially elongated by +0.15 Å (BP86) and +0.17 Å (B3LYP). DFT-optimized structures in the S=1/2 state, however, show slightly shorter bond lengths. Structural parameters calculated for the S=3/2 state deviate the least from the crystal structure and give the smallest RMSD (see above). This provides a structural argument for the assignment of the intermediate spin to be present in the crystal structure of complex **1**.

Results obtained with the BP86 functional show that in the S=3/2 state the bond distance between the iron and the axially bound sulphur atom increases compared to the low-spin by +0.16 Å and to the high-spin state by +0.05 Å. In contrast, bond lengths to the equatorial sulphur binding partners decrease by -0.15 Å (BP86). The pyramidality parameter, the out-of-plane angle <(Fe-plane), is a measure of the shift of the central iron atom out of the equatorial plane formed by the four mnt-sulphur atoms. A planar geometry would have a pyramidality value of 180°. The out-of-plane angle decreases with increasing spin multiplicity.

In BP86 calculations the <(Fe-plane) decreases from 159.4° (S=1/2), via 155.6° (S=3/2) to 146.8° (S=5/2) indicating an increase of distortion of the square-pyramidal geometry. A similar trend is observed for B3LYP calculations.

Structural parameters obtained with a B3LYP functional with reduced 10% Hartree-Fock exchange (B3LYP**) can be found in the Supplementary Material (Table S1).

Figure 3 shows a superposition of the X-ray structure of **1** and the BP86 calculated structures in each spin state. The orientation of the maleonitrile dithiolate ligands as well as that of the thiophenolate ligand in the crystal structure is best reproduced by the S=3/2 state-optimized structure using either functional. Both, the S=1/2 and S=5/2 states show larger deviations concerning the position of the thiophenolate ligand (Figure 3). With the BP86 functional, the RMSDs of only the axial thiophenolate ligand in the S=1/2, S=3/2 and S=5/2 states from the X-ray structure are 0.30 Å, 0.18 Å and 0.29 Å, respectively. This shows that both the bond distances and the orientations of the equatorial mnt and axial thiophenolate ligands are critically influenced by the spin state of the central metal atom.

For the S=3/2 state, our BP86 calculations yield structural parameters in excellent agreement with the crystal structure. Bond lengths are accurate to within 0.01 Å to 0.03 Å and bond angles were found to differ by approximately 2° and are within 1° if only

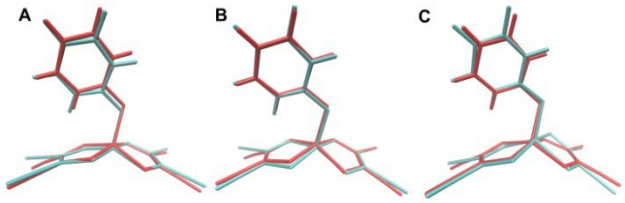


Figure 3. Superposition of the BP86/def2-TZVP-optimized structures and the crystal structure of complex **1**. Optimized structures in **A)** low-spin (S=1/2), corresponds to local minimum, **B)** intermediate-spin (S=3/2), and **C)** high-spin (S=5/2) state are shown in cyan and superposed onto the experimental crystal structure (red).

the angles between the iron atom and the equatorial sulphur atoms are considered. These results demonstrate the suitability of DFT methods for complex **1** and are slightly more accurate than calculations on the S=3/2 ground state square-pyramidal Fe(III)-$N_2S_2$ complex with one axial chloride ligand (BLYP/6-31G*).[28]

Calculations on an iron(III) square-planar complex with four equatorially bound sulphur atoms (i.e. with a vacant axial binding site) gave even larger deviations.[29] For the S=3/2 state, the calculated equatorial iron-sulphur bond lengths deviated by 0.05 Å from the X-ray structure. Our agreement of calculated structural parameters (0.01 Å for $S_{eq}$) with those from the X-ray structure give us confidence in the reliability and accuracy of the chosen computational means (functional and basis set) and the neglect of crystal packing effects when comparing with the X-ray structure of complex **1**.

## Orbital occupancies and structural parameters

To understand the influence of the spin state on the molecular geometry of a transition metal complex one has to inspect the distribution of the $d^5$ electrons over the iron d-orbitals (Figure 4). Complex **1** is a penta-coordinate complex in a square-pyramidal geometry. The occupation of the orbitals depends on the orbital energies, i.e. the energy splitting between orbitals. Early studies on square-pyramidal transition metal complexes[30] revealed that the energy levels of the 3d orbitals strongly depend on the angle between the central iron and the closest atoms of the equatorial ligand (denoted as <(Fe-plane) in Table 1). For the out-of-plane

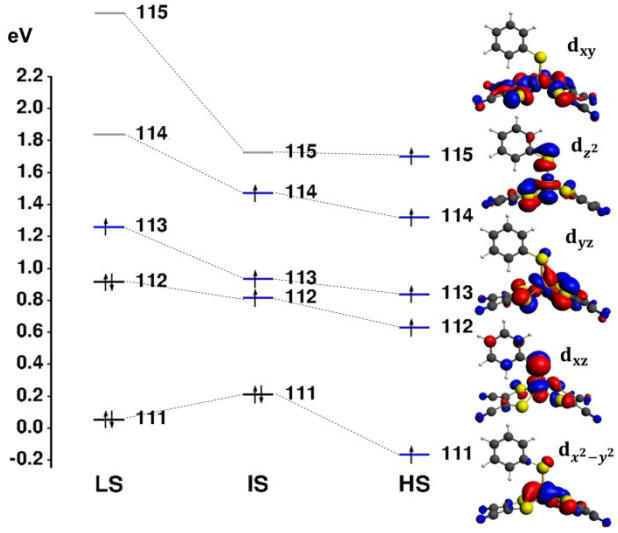


Figure 4. Calculated Fe 3d orbital splitting of complex **1** in the S=1/2 (LS), S=3/2 (IS) and S=5/2 (HS) states. Doubly occupied orbitals are shown in black, singly occupied in blue and unoccupied in grey.

angle <(Fe-plane) being smaller than 180° Rossi *et al.* assume the $d_{xy}$ orbital to be lowest in energy, followed by the $d_{xz}$ and $d_{yz}$ orbitals. The $d_{z^2}$ orbital is significantly higher in energy but still lower than the highest energy orbital, the $d_{x^2-y^2}$ orbital[30]. Our analysis of the MO energies of complex **1** gives a different ordering regarding the $d_{xy}$ and $d_{x^2-y^2}$ orbitals. The $d_{x^2-y^2}$ orbital is calculated to be lowest in energy, followed by the $d_{xz}$ orbital and the $d_{yz}$ orbital with a large splitting of about 1.0 eV (Figure 4). Rossi *et al*[30] found that the $d_{xy}$ orbital is less involved in any bonding to the ligands. The equatorial mnt ligands of complex **1** are off the x- and y-axes, therefore the $d_{xy}$ orbital obtains a strong anti-bonding character which results in destabilization and a high energy level. The $d_{x^2-y^2}$ orbital is almost non-bonding and therefore lowest in energy. The $d_{xz}$ and $d_{yz}$ orbitals are strongly involved in π-bonding and destabilized due to their participation in the anti-bonding interaction with the p-orbitals of the equatorial sulphur ligands. The $d_{z^2}$ orbital forms an anti-bonding orbital with the axial thiophenolate ligand. The major structural difference between the S=1/2 and S=3/2 states in complex **1** is the significantly elongated bond between the iron atom and the axial ligand in the intermediate-spin state (Table 1). This is due to the elevation of an electron into the anti-bonding $d_{z^2}$ orbital in the S=3/2 state, thereby weakening the metal-axial sulphur ligand bond. Similarly, when one electron is distributed to the anti-bonding $d_{xy}$ orbital in the S=5/2 state, an elongation of the bonds between the iron atom and the equatorial ligands is observed (Table 1). These structural differences are clearly consequences of the different spin states and orbital occupancies as was also shown by other groups.[28],[31],[32]

The nature of the ligands determines the d-orbital energy splitting as well as the number of ligands and their orientation. According to ligand field theory[33], the ligand strength determines the energy difference between the molecular orbitals. For penta-coordinate iron(III) porphyrins[34],[35] and heme proteins[36] it is known that the energy of the orbitals can be influenced by an increase of the field strength of the axial ligand in order to stabilize a desired spin state. The two equatorial maleonitrile dithiolate ligands (mnt) in complex **1** are rather weak-field π-donor ligands. Recent studies[31, 37] showed that the intrinsic π-electron system of the mnt ligands leads to a splitting of the otherwise degenerate $t_{2g}$ orbitals in an octahedral complex.[37] This suggests that the nature of equatorial ligands surrounding the central iron atom is of utmost importance for the electronic properties and spin state of the complex and therefore determines the suitability of a complex to be a biomimetic catalyst.

## Ordering of spin states, the effect of HF exchange and spin contamination

Both BP86 and B3LYP agree on the intermediate spin structure to have the smallest RMSD from the crystal structure and show that the low-spin and high-spin structures display some structural differences. In the following we investigated the relative energetic ordering of the different spin states of complex **1**.

Both BP86 and B3LYP calculations agree on the S=3/2 intermediate spin state to be lowest in energy (see Table 2) and are thus able to reproduce the experimentally determined ground state of complex **1**. This is in agreement with the analysis of structural parameters (see above). However, the energetic ordering of the S=1/2 and S=5/2 states varies depending on the functional employed. BP86 calculations yield the S=1/2 state to be 14 kcal/mol lower in energy than the high-spin state (S=5/2). The energy difference between the S=3/2 and S=1/2 state is small (1.1 kcal/mol), whereas the optimized S=5/2 state structure has a considerably higher energy (15.1 kcal/mol) compared to the ground

Table 2. The effect of dispersion corrections on the energy differences in kcal/mol of complex **1** (def2-TZVP basis set).

| Spin state | BP86 | BP86-D3 | B3LYP | B3LYP-D3 |
|---|---|---|---|---|
| S=1/2 | +1.1 | +0.7 | +11.6 | +11.1 |
| S=3/2 | 0 | 0 | 0 | 0 |
| S=5/2 | +15.1 | +14.7 | +2.6 | +2.3 |

state. The B3LYP functional, however, reverses the ordering of high-spin and low-spin states. It gives the S=5/2 state to be +2.6 kcal/mol above the ground state and the S=1/2 state to be highest in energy (+11.6 kcal/mol). The inclusion of dispersion correction has only a minor impact on the results, and slightly reduces the energy differences for both pure (by -0.4 kcal/mol) and hybrid functionals (by -0.3 to -0.5 kcal/mol) (see Table 2). In the following calculations, the effect of dispersive corrections was thus considered too small and not included.

It has previously been shown that a reverse energetic ordering of spin states in hybrid DFT calculations is a consequence of the amount of HF exchange admixed to the hybrid exchange-correlation functionals.[22] For standard B3LYP, the amount of HF ($c_3$) takes the value 0.2 (20%).[38] Reduction of the exact HF amount to 15% ($c_3$=0.15) results in a hybrid functional (denoted as B3LYP*[22]) that is found to perform superior for low-spin *vs.* high-spin states especially for iron(II) transition metal complexes which previously could be described only poorly using DFT. B3LYP* reproduced the experimentally derived ground state preferences (LS vs. HS) of different iron(II) octahedral complexes.[22] Hybrid functionals using between 8% and 16% of exact HF exchange give accurate results for different low-spin[39] and high-spin Fe(II)-S complexes[40] and should, in general, be preferred over pure functionals when investigating iron containing complexes. Thus, the influence of Hartree-Fock exchange on the energetic ordering of iron(III) spin states of complex **1** was also investigated here. The amount of exact exchange in the B3LYP functional was varied between 0 ($c_3$=0.0) and 30% ($c_3$=0.3) and the energy differences between ground state and the higher spin states (see Figure 5) and between low-spin and high-spin states (Table 3) were calculated.

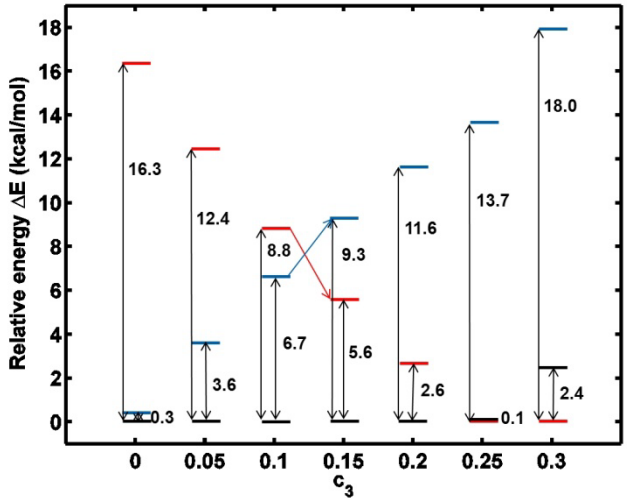


Figure 5. Relative energies ΔE in kcal/mol of complex **1** in different spin states as a function of HF exchange coefficient $c_3$ (B3LYP). Energies of S=1/2 (—), S=3/2 (—), and S=5/2 (—) are given relative to the lowest energy state (ΔE=0).

Upon variation of the amount of HF exchange, the S=3/2 spin state remains the electronic ground state of complex **1** up to almost 25% exact HF (see Figure 5). An increase of Hartree-Fock exchange leads to a preference of the high-spin state over the low-spin state. Consequently, a functional with at least 25% of Hartree-Fock exchange completely reverts the order of states and gives the S=5/2 state to be the ground state of complex **1** (this would be a IS/HS spin-crossover, see also Supplementary Material, Table S1). This contradicts the results of all of the other calculations but also the experimentally determined S=3/2 ground state. Thus, a value of $c_3 \geq 0.25$ is unsuitable for the description of the electronic structure of the present complex.

The BP86, B3LYP and B3LYP** ($0<c_3<0.25$) calculations are able to correctly reproduce the INTERMEDIATE spin as the ground state, whereas the subsequent energy ordering of LS and HS states remains unsettled. Variation of $c_3$ also has a strong effect on the relative ordering of LS and HS states. The energy splitting $\Delta E_{LS/HS}$ is shown in Table 3. For pure functionals (BP86, BLYP) and those functionals with up to 10% of HF exchange, the S=1/2 state is calculated to be lower in energy than the S=5/2 state, i.e. $\Delta E_{LS/HS}$ takes positive values. We used two functionals with 10% of HF exchange, namely the TPSSh functional and the modified B3LYP functional encoding 10% HF exchange (here termed 'B3LYP**'). Both functionals give almost identical results in $\Delta E_{LS/HS}$ splitting (2.2 and 2.7 kcal/mol). The TPSSh functional was also successfully used to investigate Fe(II) spin-crossover compounds.[41] An inverted ordering for LS and HS states, however, is obtained with functionals encoding at least 12% exact HF exchange. When investigating the energy dependence on $c_3$ of all three spin states (LS, IS, HS) (Figure 5), we find a LS/HS crossover between $c_3$=0.1 and $c_3$=0.15. Such a flipping of electronic spin states ('spin crossover') due to admixture of HF exchange was first systematically investigated by Reiher.[42] The prominent $Fe(II)(phen)_2(NCS)_2$ complex was investigated and the dependence of LS/HS transitions on the $c_3$ parameter was used as a criterion to classify transition metal complexes as 'standard' (hardly dependent on $c_3$), 'critical' ($\Delta E_{LS/HS}$ dependent on $c_3$ but not crossing the zero-splitting horizontal line) and 'complicated' ($\Delta E_{LS/HS}$ dependent on $c_3$ AND crossing the zero-splitting horizontal line). Since the slope of $\Delta E_{LS/HS}$ ($c_3$) is large, complex **1** is a spin-crossover compound with respect to LS/HS transition (i.e. is 'complicated'; see Figure 6). The situation for complex **1** is even more difficult since two spin transitions are possible. The energy splitting of both LS/HS and LS/IS transitions becomes smaller with an increasing amount of HF exchange in an almost linear fashion (Figure 6). Negative values indicate that the intermediate-spin or high-spin state is favoured over the low-spin state, respectively. The $\Delta E_{LS/IS}$ transition slope is moderate and justifies this transition to be termed 'critical'.

Our B3LYP** (10% HF) structural optimization gave accurate structural parameters (bond lengths and angles) (see Supplementary Material, Table S2 and compare with Table 1). The RMSD was 0.28 Å, thus we decided to use this functional to further investigate the influence of the axial ligand of the complex (see below). A functional with reduced HF exchange seemed plausible for studies

Table 3. $\Delta E_{LS/HS}$ in kcal/mol between the S=1/2 and S=5/2 states of complex **1** using different exchange-correlation functionals and the def2-TZVP basis set.

| Exchange-correlation functional | $\Delta E_{LS/HS}$ [a] |
|---|---|
| B3LYP ($c_3$=0.00) | 16.0 |
| BP86 | 14.0 |
| BLYP | 9.9 |
| B3LYP ($c_3$=0.05) | 8.8 |
| TPSSh (HF=10%) | 2.7 |
| B3LYP** ($c_3$=0.10) | 2.2 |
| B3LYP ($c_3$=0.12) | -0.3 |
| B3LYP ($c_3$=0.13) | -1.5 |
| B3LYP* ($c_3$=0.15) | -3.8 |
| B3LYP ($c_3$=0.20) | -9.0 |
| B3LYP ($c_3$=0.25) | -13.7 |
| B3LYP ($c_3$=0.30) | -18.0 |

[a] A positive value of $\Delta E_{LS/HS}$ indicates that the low-spin state (S=1/2) is lower than the high-spin state (S=5/2).

on iron-sulphur cluster DFT calculations. Szilagyi *et al.*[43] investigated the performance of different functionals for iron-sulphur clusters. When using a functional encoding 5% HF exchange and the Perdew86 correlation[44], they obtained structural parameters in good agreement with experiment (bond lengths within 0.03 Å), however, atomic spin densities were found to differ from XAS studies.

The B3LYP** functional was also used for structural parameters and IR and UV/vis spectra of an iron(II) spin crossover compound and gave results in good agreement with experiment.[26]
Harvey and Aschi investigated the energetics of the $Fe(CO)_5$ complex using different pure and hybrid functionals.[47] They modified the amount of exact exchange in the B3PW91 functional and obtained the B3PW91* ($c_3$=0.15) and B3PW91** ($c_3$=0.10) functionals. They observed an increasing energy splitting between singlet and triplet states with larger amounts of exact HF exchange. Taking CCSD(T) calculations with BP86 DFT optimized orbitals as a reference and extrapolating to larger basis sets, Harvey and Aschi obtained the B3PW91* functional with 15% HF exchange to come closest to the reference splitting.

For complex **1**, spin contaminations for the BP86 and B3LYP functionals as well as the B3LYP functional with different $c_3$ values are given in the Supplementary Material (Table S3). For pure functionals spin contamination is less relevant than for hybrid functionals. Spin contamination increases with the amount of HF exchange and leads to deviations of up to 100% for $c_3$=0.3 in the S=1/2 spin state.

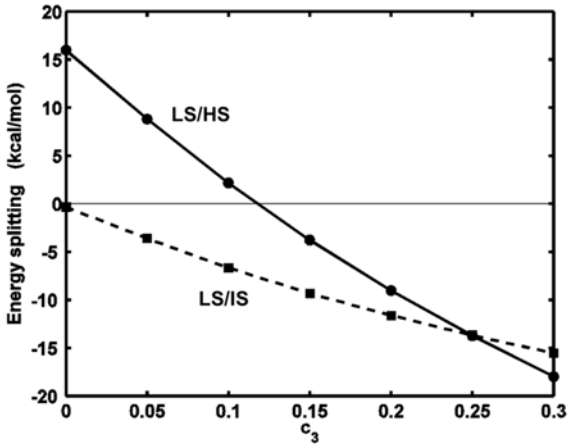


Figure 6. Energy splitting between the S=1/2 and S=3/2 states (dashed line) and the S=1/2 and S=5/2 states (solid line) as a function of the amount of HF exchange $c_3$ in the B3LYP functional.

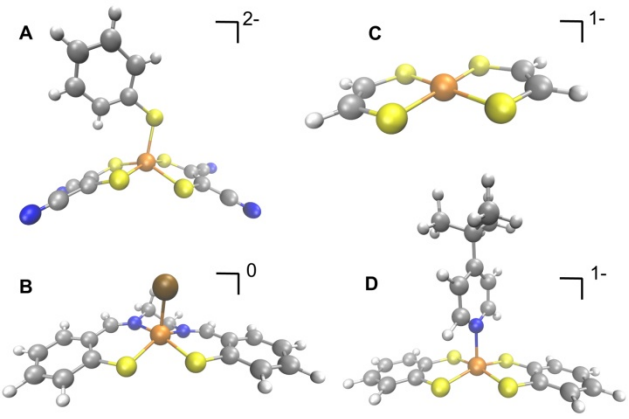


Figure 7. Iron(III) complexes found to exhibit a quartet ground state include **A)** complex **1**, **B)** chloro(N,N'-ethylenebis(mercaptosalicylidene-iminato) iron(III)[28],[45], **C)** an iron bis(dithiolene) model complex[29], and **D)** bis(benzene-1,2-dithiolato)iron(III)-4-tert-butylpyridine[46].

For complex **1**, the S=3/2 state was unequivocally shown to be the ground state. Such an intermediate spin ground state was also found for other iron(III) compounds (see Figure 7). For example, Chang *et al.*[28],[45] described a square-pyramidal iron(III) complex with iron(III) surrounded by two equatorially bound sulphur and two nitrogen atoms as well as an axial chloride ligand (Figure 7B). Another square-planar iron(III) complex (Figure 7C)[29] was also found to exhibit a quartet ground state. Investigating redox-noninnocent S,S'-coordinated benzene-1,2-dithiolate ligands, Ray *et al.*[46] described a penta-coordinate iron(III) complex with intermediate ground state (Figure 7D). In this case the S=3/2 state was determined by EPR and Mössbauer spectroscopy. A series of square-pyramidal penta-coordinate $S_4$ iron(III) complexes with four equatorially bound sulphur atoms and one axial halide ligand (Cl, Br, I) was also found to exhibit a S=3/2 ground state.[48]

In addition, iron atoms surrounded by four sulphur atoms in a plane and one axial nitrogen atom are found in octahedral iron(II) complexes. The ground state described for those complexes is, depending on the sixth ligand, either the low-spin[39] or the high-spin[40] state. Porphyrins, a group of penta-coordinate iron(III) complexes in which the iron atom is surrounded by four equatorial nitrogen atoms and one axially bound ligand, are found to exhibit a high-spin ground state when the axial ligand is anionic.[49] There are, however, also reports about intermediate spin (S=3/2) iron(III) porphyrinato complexes.[50]

## Torsional profile of the orientation of the axial ligand

In the crystal structure of complex **1**, the axial thiophenolate ligand is located above one of the mnt ligands (Figure 1B). The torsional profile of the thiophenolate ligand was investigated in order to probe the accessibility of other rotational conformers in solution and during the proton reduction pathway. The thiophenolate ligand was rotated by 180° in steps of 5° around the $S_{ax}$-Fe-$S_{eq}$ angle (see Figure 8) and each structure was energy minimized (Figure 8 and Supplementary Material, Table S4). A rotation of 180° covers all possible structures due to the two-fold symmetry of complex **1**. Figure 8 shows the torsional profile for our BP86 calculations in the gas phase, with dispersion correction and in solution for the intermediate spin S=3/2 and the low-spin S=1/2 states. The torsional profile for the high-spin S=5/2 state is very similar to the S=3/2 state and not shown. We already showed that the position of the axial ligand in the crystal structure corresponds to the lowest energy orientation in the S=3/2 and S=5/2 state structures. Vibrational analysis of these orientations gave only positive frequencies, thereby proving them to be minima. DFT calculations in the gas phase, with dispersion correction and in acetonitrile are found to give a similar qualitative behaviour.

For the S=3/2 state, rotation of the axial ligand has a barrier of +3.8 kcal/mol in the gas phase. Dispersion correction increases the rotational energy barrier by 1.4 kcal/mol to a value of +5.2 kcal/mol. In acetonitrile the energy barrier was +4.4 kcal/mol. The Gibbs free energy difference at 298 K between the starting conformation and the highest energy structure is 4.6 kcal/mol (BP86) for the S=3/2 state. In B3LYP gas phase calculations (data not shown), the energy differences are smaller compared to the BP86 calculations (+1.9 kcal/mol). The energetically most unfavourable orientation of the thiophenolate ligand is found for a perpendicular rotation (by θ=90°) from the initial structure (θ=0°). This orientation (θ=90°) was proven to be a transition state featuring exactly one imaginary frequency.

For the S=1/2 state, however, an inverted torsional profile was found (see Figure 8). The initial position of the thiophenolate ligand in the crystal structure is a local but not the global minimum (absence of imaginary frequencies could be shown). The global minimum structure is obtained when the ligand orientation was nearly perpendicular (θ=75°) to the starting conformation. This ligand orientation is lower in energy by 3.3 kcal/mol in the gas phase, 1.9 kcal/mol with dispersion correction and 3.0 kcal/mol in acetonitrile. Here, dispersion correction has the effect of reducing the perpendicular ligand orientation preference compared to the gas phase. The Gibbs free energy for the perpendicular ligand orientation at 298 K is lower by 2.9 kcal/mol (BP86) compared to the starting conformation. Both global minima structures are shown in Figure S1 (Supplementary Material). Both structures are stabilized by hydrogen bonds between the equatorial sulphur atoms and the thiophenolate hydrogen atoms, which are expected to form in both states irrespective of the nature of electron pairing. However, different orbital occupancies serve as an explanation for the distinctive favoured orientation in the low-spin state versus the intermediate-spin and high-spin states. In contrast to the S=1/2 state, we found the $d_{z^2}$ orbital to be filled with one electron in the higher spin states (see Figure 4). The iron $3d_{xz}$ orbital is doubly occupied in the S=1/2 state and the overlap with the 3p orbitals of the sulphur atoms of the thiophenolate ligand is energetically most favourable in a perpendicular orientation of the ligand.

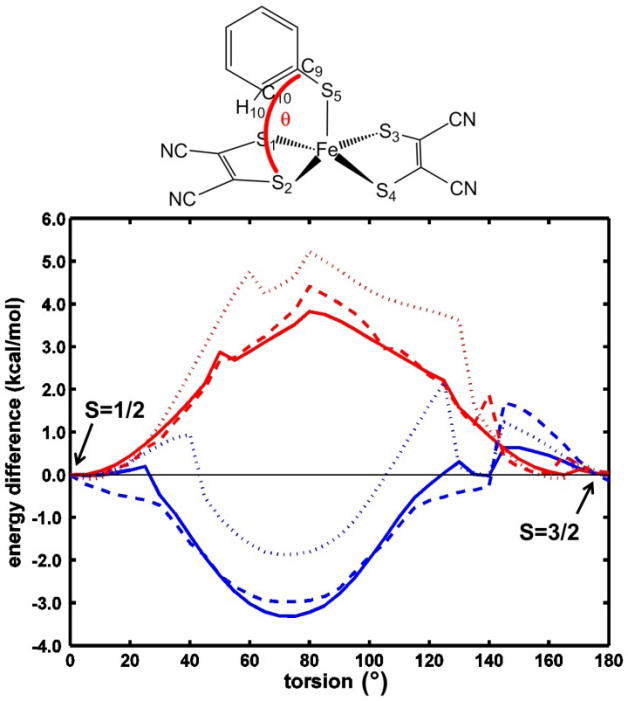


Figure 8. Torsional profile of the axial thiophenolate ligand rotation. During the potential energy scan the axial thiophenolate ligand was rotated around the torsion angle θ ($S_2$-Fe-$S_5$-$C_9$). Relative energies in kcal/mol for the S=1/2 state (blue) and the S=3/2 state (red), for BP86 in gas phase (solid line), BP86-D3 with dispersion correction (dotted line) and in acetonitrile (dashed line). The highlighted orientations correspond to the local minimum structures shown in Table 1.

In all investigated torsional profiles there are significant structural fluctuations between θ=135° and 150°. We observe a flipping of the axial thiophenolate ligand due to hydrogen bond formation to one sulphur atom of the maleonitrile dithiolate. Thus, the local higher energy conformers between θ=135° and θ=150° correspond to a structure where one hydrogen atom of the thiophenolate ligand closely approaches the sulphur atom of the maleonitrile ligand and then a ligand orientation flip occurs (for details see Supplementary Material, Figure S2). Our calculations show that the spin state of the iron has an effect on the preferred orientation of the axial ligand. In the intermediate- and high-spin states, the global minimum is the one obtained from X-ray structural analysis. In the low-spin state, however, the global minimum has a perpendicular axial ligand orientation. The barriers to rotation are higher than thermodynamic corrections at room temperature but the involvement of different conformation states during the catalytic process has to be considered.

The global S=1/2 minimum (see Table S7 and Figure S1, Supplementary Material) is lower in energy than the global S=3/2 minimum when the BP86 functional is used. However, the hybrid functionals B3LYP** and B3LYP give the S=3/2 state as the ground spin state. Consideration of thermal corrections and entropy favours the S=5/2 state over the S=1/2 state (see below).

## Influence of the nature of ligands on the ordering of spin states

In order to examine the influence of the axial ligand on the preferred ground state, several axial ligands were investigated (Table 4, Figure 9). Removal of the axial ligand (complex **2**) gave a square-planar Fe(III)$(mnt)_2^-$ complex with a S=3/2 ground spin state for all functionals investigated. This was also found by Jacobsen *et*

Table 4. Relative Gibbs free energy differences ΔG (298 K) in kcal/mol between different spin states for Fe(III)$(mnt)_2$X.

| ligand X | $SPh^-$ (1) | | | Vacant (2) | | | $CN^-$ (3) | | | CO (4) | | |
|---|---|---|---|---|---|---|---|---|---|---|---|---|
| Spin state | BP86 | B3LYP** | B3LYP | BP86 | B3LYP** | B3LYP | BP86 | B3LYP** | B3LYP | BP86 | B3LYP** | B3LYP |
| S=1/2 | +2.5 | +7.7 | +12.6 | +3.7 | +5.4 | +8.2 | 0 | 0 | +4.3 | 0 | 0 | +0.5 |
| S=3/2 | 0 | 0 | 0 | 0 | 0 | 0 | +11.3 | +3.8 | 0 | +20.5 | +11.0 | 0 |
| S=5/2 | +12.9 | +7.2 | +1.6 | +16.9 | +12.2 | +6.6 | +24.3 | +11.1 | +1.8 | +41.8 | +27.1 | +10.9 |

*al.*[29] Compared to complex **1**, we observed some quantitative changes in the relative energies and the ordering of higher spin states. For both BP86 and B3LYP** calculations the energy difference between the S=3/2 and S=1/2 states is still small, +3.7 kcal/mol and +5.4 kcal/mol, respectively (Table 4).

The S=5/2 state is highest in energy with +16.9 kcal/mol (BP86) and +12.2 kcal/mol (B3LYP**) above the ground state. The B3LYP functional decreases the Gibbs energy difference to the high-spin state and gives the S=5/2 state +6.6 kcal/mol above the S=3/2 state followed by the S=1/2 state with +8.2 kcal/mol. An energy difference of 3.7 kcal/mol (BP86) between the S=3/2 and S=1/2 states is larger than the value obtained by Jacobsen *et al*.[29] Using also the BP86 functional Jacobsen *et al*. found the S=3/2 state to be lower in energy than the S=1/2 state by 1.7 kcal/mol for a planar iron(III) complex (see Figure 7C). Our complex **2** features cyanide ligands instead of hydrogen atoms. Apparently, even the nature of the equatorial ligands and terminal ligand atoms strongly influence the energy levels of the central metal orbitals and therefore the energies of the spin states of the complex. Complexes **3** and **4** with an axial cyanide or carbonyl ligand, are examples for strong field ligand complexes. In these cases, the interaction between the central iron(III) atom and the ligand is strong; therefore it is energetically favourable to rather pair electrons than to occupy orbitals with higher energy.[33]

As a consequence, complexes involving a cyanide or phosphine ligand are often low-spin complexes.[51] We thus expected the S=1/2 state to be the ground state of both complexes **3** and **4**. Both BP86 and the modified B3LYP** give the low-spin state to be the ground state of complex **3**, indeed. The original B3LYP functional, however, still yields an S=3/2 ground state. With BP86 and B3LYP**, the S=1/2 state is the most favourable state followed by

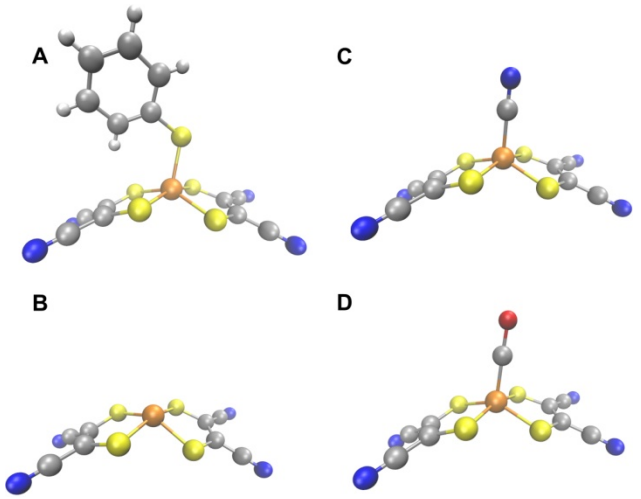


Figure 9. **A)** Complex **1**, **B)** vacant axial site (complex **2**), or axial ligand substitution by **C)** a cyanide ligand ($CN^-$, complex **3**) or **D)** a carbonyl ligand (CO, complex **4**).

the S=3/2 and S=5/2 states; with BP86, each state is characterised by a large energy splitting of more than 10 kcal/mol. The standard B3LYP functional ($c_3$=0.20) for complex **3** provides qualitatively similar results compared to complex **1** but with a much smaller energy difference between the S=1/2 state and S=3/2 ground state (approximately +4 kcal/mol). Similarly, for complex **4** with an axial carbonyl ligand the BP86 and B3LYP** functionals predict the S=1/2 state to be lowest in energy, followed by the S=3/2 and S=5/2 states. The S=3/2 state is +20.5 kcal/mol or +11.0 kcal/mol above the ground state for BP86 and B3LYP**, respectively. The high spin states are well separated in energy by +41.8 kcal/mol (BP86) and +27.1 kcal/mol (B3LYP**) from the low-spin ground state. The B3LYP functional gives a different picture: the S=3/2 state is the complex' ground state followed by the S=1/2 (+0.5 kcal/mol) and S=5/2 (+10.9 kcal/mol) states. Thus, the pure BP86 functional and the B3LYP** functional are able to give the expected ground states of complexes **3** and **4** but not the original B3LYP functional. The carbonyl and the cyanide ligand are isoelectronic and known to be weak σ-donors and a strong π-acceptors.[33] A natural population analysis (see Supplementary Material, Table S5) of the complexes **1**, **3**, and **4** reveals that the differences between the atomic partial charges increase with an increasing spin multiplicity, i.e. the charge distribution within the molecule is less delocalized and becomes more ionic for higher spin states. In particular for the iron atom, the partial charge becomes more positive for higher spin multiplicities, e.g. from +0.14 in the S=1/2 state to +0.87 in the S=5/2 state for complex **1**. In contrast, the sulphur atoms in the equatorial plane become more negative (i.e. from 0.00 to -0.16 in complex **1**). This effect can be explained by the increase of π back-donation of charge from the metal to the ligands. In the S=1/2 state, the carbon atoms of the axial ligands $CN^-$ and CO in complexes **3** and **4** exhibit a positive partial charge (+0.11 and +0.25, respectively). The d-orbital splitting is large, and a low spin ground state is obtained. In contrast to the CO and $CN^-$ ligand, the $SPh^-$ in complex **1** exhibits a different charge distribution. The sulphur atom carries a negative charge. This leads to a larger Fe-S bond distance and weaker interaction with the metal. As a consequence, $SPh^-$ causes a smaller iron d-orbital splitting, i.e. is a weaker ligand compared to CO or $CN^-$, and complex **1** adopts the intermediate-spin (S=3/2) state.

## Thermodynamic corrections, spin-crossover and critical temperature $T_C$

The pronounced spin-state dependence on the admixture of HF exchange (see Figure 6) and the small Gibbs energy differences between the spin states (see Table 4) prompted us to investigate whether complex **1** belongs to the group of spin crossover compounds. The phenomenon of thermal spin crossover is mainly described for hexa-coordinate iron(II) complexes that show the transition from the low-spin (S=0) to the high-spin (S=2) state in answer to a physical stimulus, for reviews see for example [27],[52],[53].

The spin crossover phenomenon is described in solid state as well as in solution. However, in solution, the thermal spin crossover is not an effect of intermolecular cooperativity as it is in solid state systems.[24],[25] The spin crossover is driven by an entropy increase accompanying the transition from low-spin to high-spin state. Cooperative interactions that are based on electron-phonon coupling associated with spin transition in adjacent molecules are important in the solid state. These effects of cooperativity cannot be

taken into account using the isolated-molecule approach in DFT calculations.[42]

First, we investigated the spin state ordering dependence when applying thermodynamic corrections. So far, we compared energetic differences only and did not include thermic and entropic corrections. The Gibbs free energy differences of the spin states as a function of the amount of exact HF exchange in the hybrid B3LYP functional are shown in Table S6 (Supplementary Material). The S=3/2 state remains the thermodynamic ground state for complex **1** between 0 K and room temperature (see Table 2 and Table S6).

The low-spin/high-spin (LS/HS) transition, however, is found to be both temperature- and HF exchange-dependent. At 0 K (Table 2), the S=5/2 state is lower in energy than the S=1/2 state when $c_3$>0.12. In contrast, at room temperature the S=5/2 is favoured over the S=1/2 state with functionals with at least 10% of HF exchange (Table S6) due to entropic contributions. Therefore, $\Delta G_{LS/HS}$ (298 K) between the S=1/2 and the S=5/2 state is always smaller than the corresponding $\Delta E_{LS/HS}$ (0 K), e.g. $\Delta E_{LS/HS}$=+2.2 kcal/mol and $\Delta G_{LS/HS}$=-0.5 kcal/mol for the B3LYP** functional. Entropic contributions to spin transitions and the Gibbs energy differences were analysed for the LS/HS transition in the $Fe(phen)_2(NCS)_2$ complex as an example.[54],[55] B3LYP and even B3LYP* were shown to fail for $Fe(phen)_2(NCS)_2$ and gave a high-spin ground state.[42] Swart[56] used the OPBE functional[57] to obtain the true low-spin ground state with the high-spin state +2.1 kcal/mol (at 0 K) higher in energy. This is in very good agreement with the experimentally derived value of $\Delta E$=+1.8 kcal/mol.[56] The B3LYP** functional also reproduced the low-spin ground state (data not shown).

The difference in entropy between the low-spin and high-spin state is due to three contributions, namely an electronic, vibrational and rotational contribution. For the spin crossover compound $Fe(phen)_2(NCS)_2$ the high-spin to low-spin transition is associated with a shifting of the C-N and C-S stretching modes due to an increased metal-ligand bond strength.[58] Since the LS/HS transition is characterised by the transfer of two electrons to high-energy orbitals, the molecular geometry is significantly affected, thereby also altering the stretching vibrations. This is also found for complex **1** as in the S=5/2 state the metal-ligand bonds are considerably elongated compared to the S=1/2 state (Table 1). The calculated Fe-$S_{ax}$ stretching vibration is 334 $cm^{-1}$ in the S=1/2 state, 341 $cm^{-1}$ in the S=3/2 state, and 344 $cm^{-1}$ in the S=5/2 state for B3LYP** calculations. For BP86 we found Fe-$S_{ax}$ stretching vibrations of 346 $cm^{-1}$ (S=1/2), 326 $cm^{-1}$ (S=3/2), and 339 $cm^{-1}$ (S=5/2). It was expected that the elongation of the Fe-$S_{ax}$ bond is associated with a decrease of the corresponding vibrational frequency. This trend could only be observed for pure BP86 calculations. B3LYP** and B3LYP calculations failed to give the correct decrease in vibrational frequencies for increasing bond length between the iron centre and the axial sulphur atom (data not shown). Rackwitz et al.[59] investigated the cooperative behaviour of metal centres in spin crossover iron(II) complexes by DFT calculations. They found that the elongation of the metal-ligand bond results in an increase of the vibrational entropy. On the other hand, the vibrational energy slightly decreases when the low-spin state changes into the high-spin state.[59] In total, these two effects add up to a lowering of the Gibbs free energy for the high-spin

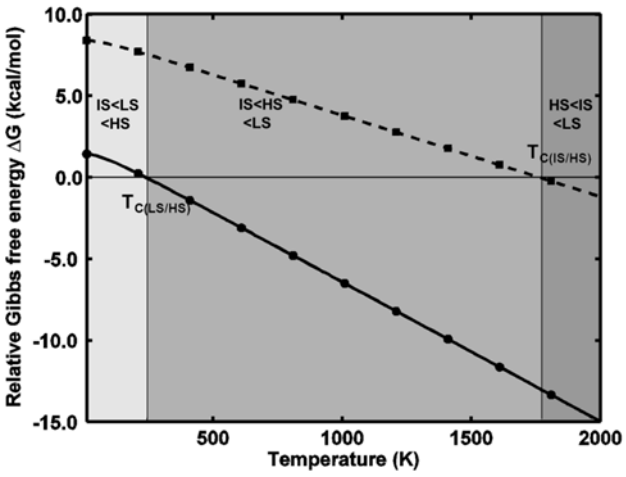


Figure 10. Spin transitions and critical temperatures $T_C$. The Gibbs free energy differences $\Delta G_{LS/HS}$ (solid line) and $\Delta G_{IS/HS}$ (dashed line) as a function of the temperature (B3LYP**, def2-TZVP).

relative to the low-spin state. Kepp *et al.* published data to show that the ZPE, thermal corrections as well as the entropy favour the high-spin state of different iron(III) porphyrin complexes.[60] Similarly they argue that these effects origin from the longer and weaker metal-ligand bonds in the high-spin state which allow higher vibrational entropic contributions compared to the low-spin state. The difference in the Gibbs free energies between the different spin states is dependent on temperature T and shown in Figure 10 and Table S8 for the B3LYP** functional (Supplementary Material). The lines in Figure 10 display the temperature dependence of the LS/HS and IS/HS transition course associated with Gibbs free energy differences. We define a critical temperature, $T_C$, that marks the point for the LS/HS transition or IS/HS transition, respectively. This 'temperature' $T_C$ is only used as a relative probe for the accessibility of spin transitions of isolated molecules and does not consider solid state interactions, cooperativity or phase transitions.

Below $T_{C(IS/HS)}$=1760 K we find that the S=3/2 state is favoured over the S=5/2 state (see positive values in Figure 10). Only at temperatures above $T_{C(IS/HS)}$=1760 K the S=5/2 state becomes the ground state of complex **1**. The low-spin state remains lower in energy than the high-spin state for temperatures below $T_{C(LS/HS)}$<240 K, above which the state ordering inverts. The entropy is positive and slightly larger for the S=5/2 state than for the S=1/2 state (Table S8). Thus $\Delta S_{LS/HS}$ increases with higher temperatures. The enthalpy H is lower for the S=1/2 state compared to the S=5/2 state and increases with higher temperatures. The low-spin state never becomes the ground state of complex **1**. In order to experimentally confirm our findings regarding the thermal spin-crossover of complex **1** temperature-dependent Mössbauer spectroscopy and magnetic susceptibility measurements are necessary. However, due to the high $T_C$ of 1760 K the S=5/2 state of complex **1** is not accessible and has no relevance regarding catalysis.

The LS/HS and IS/HS transitions of complex **1** obtained with the BP86 and TPSSh functionals are shown in Figure S3 (Supplementary Material). With the BP86 functional the S=3/2 state remains the electronic ground state of complex **1** throughout all calculated temperatures. Compared to the low-spin (S=1/2) state the high-spin (S=5/2) state becomes lower in energy above a critical temperature of $T_C$=1210 K. The hybrid TPSSh functional gives results in qualitative agreement with the B3LYP** functional. We observe two critical temperatures for spin transitions. The LS/HS transition occurs at $T_C$=300 K above which the S=3/2 ground state

is followed by the S=5/2 state and the S=1/2 state even higher in energy. The S=5/2 state becomes the complex' ground state above a temperature of $T_C$=1430 K.

Mossin *et al.*[61] described the phenomenon of the IS/HS transition for a trigonal bipyramidal iron(III) complex. Using different experimental techniques including variable-temperature Mössbauer and X-band EPR spectroscopy, as well as DFT calculations they found a low symmetry complex with the S=3/2 ground state for low temperatures, whereas above 80 K the S=5/2 state was favoured. In agreement with our findings, the IS/HS crossover was associated with significant structural changes concerning the axially iron-bound ligands. Mossin *et al.*[61] assign the structural distortions as the origin of the spin transition resulting in a stabilization and occupation of the $d_{z^2}$ orbital in the high-spin state.

## Conclusions

$[Fe^{III}\text{-}(mnt)_2(SPh)]^{2-}$ is a functional mononuclear proton reducing catalyst. The structural and electronic properties of this penta-coordinate iron(III) dithiolene complex were investigated in detail using density functional theory calculations. Structural data were reproduced to within 0.03 Å and 2.3°. Prior to the present study the S=3/2 spin state was identified by EPR experiments to be the complex' electronic ground state. These experimental findings could clearly be confirmed by our calculations using both pure and various hybrid functionals. The energetic ordering of higher spin states, however, was dependent on the exchange-correlation functional. The B3LYP functional gave structural parameters in less accurate agreement with experiment. This was also found in other studies which questioned the suitability of the hybrid B3LYP functional for transition metal-containing complexes.[22],[56],[62] Generally, BP86 calculations were found to rather stabilize the low-spin state, whereas B3LYP prefers the high-spin state.[22] This supports our findings obtained for the present complex **1**. Variation of the amount of HF exchange encoded in the B3LYP functional gave a functional (B3LYP** with 10% HF exchange) that was found to perform well for complex **1**. Furthermore, the electronic effects of the axial ligands CO and $CN^-$, which are expected by ligand field theory to enforce a low-spin state, were correctly predicted.

Based on structural and energetic criteria, we clearly identified complex **1** to be a penta-coordinate mononuclear iron(III) biomimetic catalyst with an intermediate electronic ground state. Structural properties of complex **1** were found to be dependent on the iron(III) spin state. The increase in bond lengths between the iron(III) and the axially bound sulphur ligand supports the S=3/2 state and is a consequence of the 3d orbital occupancy of the central iron atom. In contrast, in the intermediate-spin state Fe-S bonds to the equatorially bound sulphur atoms are considerably shortened compared to the high-spin state. These structural properties are suitable to identify the intermediate-spin state as the state of the system corresponding to the X-ray structure (determined at low temperature 100 K).

Not only the metal-ligand bond distances but also the axial ligand orientation was found to be spin-state dependent. Complex **1** shows a spin-state thiophenolate ligand torsional angle dependent energy profile. For the S=3/2 and S=5/2 states the preferred ligand orientation was central above one maleonitrile dithiolate ligand in both gas phase and acetonitrile. In contrast, the low-spin S=1/2 state exhibits an inverted torsional profile with the lowest energy when the axial ligand is rotated by approximately 90° from the X-ray structure. As a consequence, a different orientation and geometry in solution may result in different chemical reactivity. The reactivity of complex **1** towards electrochemical proton reduction at mild overpotentials prompts the investigation of possible spin crossovers and the reactivity on different spin-state potential energy surfaces.

The selection of ligands which push the system towards a selected spin multiplicity could be a starting point for a purpose-oriented synthesis of complexes with desired electronic properties that may result in the generation of highly efficient catalysts for electrochemical proton reduction.

## Computational Details

All calculations were performed using TURBOMOLE V6.4.[63] Structural optimizations were performed at the spin-unrestricted level (UKS). The starting coordinates were taken from the crystal structure of complex **1** (CCDC-840514).[8] The performances of a pure GGA (BP86)[64],[44] and a hybrid functional (B3LYP) were compared. The B3LYP functional[65],[38],[66] is based on Becke's 1988 functional[64], which includes Slater exchange, $E_x^{LSDA}$, mixed with 20% of exact HF exchange, $E_{ex.ex}$, and combined with the Lee-Yang-Parr (LYP)[67], $E_c^{LYP}$, and VWN[65], $E_c^{VWN}$, correlation functionals.

$$E_{xc}^{B3LYP} = E_x^{LSDA} + c_1 E_x^{88} + c_2 E_c^{LYP} + (1 - c_2) E_c^{VWN} + c_3 [E_{ex.ex} - E_x^{LSDA}]$$

The coefficients $c_1$, $c_2$ and $c_3$ are set to values 0.72, 0.81 and 0.20, respectively.[22] The amount of HF exchange in the B3LYP functional was varied from zero to 30%. For comparison, energies were also calculated with the BLYP[64],[67] and the largely non-empirical hybrid TPSSh functional[68], the latter incorporating 10% HF exchange. Calculations with pure functionals were accelerated with the RI approximation.[69] A split-valence basis set of triple zeta quality (def2-TZVP) was applied to all atoms.[70] Where indicated, an empirical dispersion correction based on the approach of Grimme (DFT-D3) was used to consider van der Waals interactions.[71] In order to take solvent effects into account, additional DFT calculations were performed using the conductor-like screening model (COSMO)[72] with ε=37.5 for the simulation of an acetonitrile solvent. All structures were characterised as minima by proving the absence of imaginary frequencies. Gibbs free energies were calculated at 298 K and standard pressure (unless otherwise specified) from an analysis of the vibrational frequencies. Translational, rotational and vibrational contributions to the enthalpy and entropy were considered according to standard thermodynamic approaches (for details see[73]). The electronic contributions to the entropy were calculated and considered negligible for our results.

Thermal corrections were calculated according to the following equation:

$$E_{thermal} = ZPE + 3RT + \sum_i e(i) \cdot \left( \frac{1 + \exp\left(\frac{-e(i)}{kT}\right)}{2} \right) \cdot \left(1 - \exp\left(\frac{-e(i)}{kT}\right)\right)$$

The enthalpy was calculated according to

$$H = E_{0K} + E_{thermal} + RT$$

The entropy is

$$S = \frac{E_{thermal} + RT - chem.pot.}{T}$$

The Gibbs free energy is given by

$$G = H - S \cdot T$$

A natural population analysis (NAO analysis)[74] was performed in order to determine atomic partial charges.

The torsional profile of the axial ligand was investigated by performing relaxed potential energy surface scans at the BP86/def2-TZVP level. The torsion angle θ (Figure 8) was varied in steps of 5° while all other degrees of freedom were left unconstrained. θ=0° corresponds to the torsion angle found in the X-ray structure and scans up to θ=180° were performed.

**Supporting Information** (see footnote on the first page of this article): Further details on the performance of the B3LYP** functional, spin contamination, and energies of the torsional profile.

## Acknowledgments

We thank the Max Planck Society for the Advancement of Science and the Excellence Initiative "Research Centre Dynamic Systems: Biosystems Engineering" by the Federal State of Saxony-Anhalt for financial support.

[1] R. Cammack, M. Frey, R. Robson, *Hydrogen As a Fuel: Learning from Nature*, CRC Press, London, **2001**.

[2] R. Schlögl, *Chemical Energy Storage*, Walter de Gruyter GmbH, Berlin/Boston, **2013**.

[3] P. M. Vignais, A. Colbeau, *Curr. Issues Mol. Biol.* **2004**, *6*, 159-188.

[4] P. M. Vignais, B. Billoud, J. Meyer, *FEMS Microbiol. Rev.* **2001**, *25*, 455-501.

[5] E. C. Hatchikian, N. Forget, V. M. Fernandez, R. Williams, R. Cammack, *Eur. J. Biochem.* **1992**, *209*, 357-365.

[6] J. W. Peters, W. N. Lanzilotta, B. J. Lemon, L. C. Seefeldt, *Science* **1998**, *282*, 1853-1858.

[7] J. C. Fontecilla-Camps, A. Volbeda, C. Cavazza, Y. Nicolet, *Chemical reviews* **2007**, *107*, 4273-4303.

[8] A. Begum, S. Sarkar, *European Journal of Inorganic Chemistry* **2012**, 40-43.

[9] M. Winkler, S. Kawelke, T. Happe, *Bioresource technology* **2011**, *102*, 8493-8500.

[10] A. L. De Lacey, V. M. Fernandez, M. Rousset, R. Cammack, *Chemical reviews* **2007**, *107*, 4304-4330.

[11] a) A. Silakov, B. Wenk, E. Reijerse, W. Lubitz, *Physical chemistry chemical physics : PCCP* **2009**, *11*, 6592-6599; b) Ö. F. Erdem, M. Stein, S. Kaur-Ghumaan, E. J. Reijerse, S. Ott, W. Lubitz, *Chemistry – A European Journal* **2013**, *19*, 14566-14572; c) Y. Nicolet, A. L. de Lacey, X. Vernede, V. M. Fernandez, E. C. Hatchikian, J. C. Fontecilla-Camps, *Journal of the American Chemical Society* **2001**, *123*, 1596-1601.

[12] S. Tschierlei, S. Ott, R. Lomoth, *Energy Environ. Sci.* **2011**, *4*, 2340-2352.

[13] G. A. N. Felton, C. A. Mebi, B. J. Petro, A. K. Vannucci, D. H. Evans, R. S. Glass, D. L. Lichtenberger, *J. Organomet. Chem.* **2009**, *694*, 2681-2699.

[14] C. Mealli, T. B. Rauchfuss, *Angew. Chem.-Int. Edit.* **2007**, *46*, 8942-8944.

[15] S. Kaur-Ghumaan, L. Schwartz, R. Lomoth, M. Stein, S. Ott, *Angew. Chem.-Int. Edit.* **2010**, *49*, 8033-8036.

[16] M. Beyler, S. Ezzaher, M. Karnahl, M. P. Santoni, R. Lomoth, S. Ott, *Chem. Commun.* **2011**, *47*, 11662-11664.

[17] W. Kaim, B. Schwederski, *Coord. Chem. Rev.* **2010**, *254*, 1580-1588.

[18] R. Eisenberg, *Coord. Chem. Rev.* **2011**, *255*, 825-836.

[19] K. D. Karlin, E. I. Stiefel, *Progress in Inorganic Chemistry, Dithiolene Chemistry: Synthesis, Properties, and Applications*, Wiley, **2004**.

[20] C. J. Cramer, D. G. Truhlar, *Physical chemistry chemical physics : PCCP* **2009**, *11*, 10757-10816.

[21] F. Neese, *J Biol Inorg Chem* **2006**, *11*, 702-711.

[22] M. Reiher, O. Salomon, B. A. Hess, *Theor. Chem. Acc.* **2001**, *107*, 48-55.

[23] J. N. Harvey, *Struct. Bond.* **2004**, *112*, 151-183.

[24] P. Gutlich, A. Hauser, H. Spiering, *Angew. Chem.-Int. Edit. Engl.* **1994**, *33*, 2024-2054.

[25] P. Gutlich, Y. Garcia, H. A. Goodwin, *Chem. Soc. Rev.* **2000**, *29*, 419-427.

[26] I. Respondek, L. Bressel, P. Saalfrank, H. Kampf, A. Grohmann, *Chem. Phys.* **2008**, *347*, 514-522.

[27] P. Koningsbruggen, Y. Maeda, H. Oshio, in *Spin Crossover in Transition Metal Compounds I, Topics in Current Chemistry, Vol. 233* (Eds.: P. Gütlich, H. A. Goodwin), Springer Berlin Heidelberg, **2004**, pp. 259-324.

[28] C. H. Chang, A. J. Boone, R. J. Bartlett, N. G. J. Richards, *Inorganic Chemistry* **2004**, *43*, 458-472.

[29] H. Jacobsen, J. P. Donahue, *Inorganic Chemistry* **2008**, *47*, 10037-10045.

[30] A. R. Rossi, R. Hoffmann, *Inorganic Chemistry* **1975**, *14*, 365-374.

[31] D. Harris, G. H. Loew, A. Komornicki, *J. Phys. Chem. A* **1997**, *101*, 3959-3965.

[32] J.-P. Simonato, J. Pécaut, L. Le Pape, J.-L. Oddou, C. Jeandey, M. Shang, W. R. Scheidt, J. Wojaczyński, S. Wołowiec, L. Latos-Grażyński, J.-C. Marchon, *Inorganic Chemistry* **2000**, *39*, 3978-3987.

[33] C. J. Jones, in *d- and f-Block Chemistry* (Ed.: E. W. Abel), The Royal Society of Chemistry, **2002**, pp. 97-129.

[34] H. Keutel, I. Käpplinger, E. G. Jäger, M. Grodzicki, V. Schünemann, A. X. Trautwein, *Inorganic Chemistry* **1999**, *38*, 2320-2327.

[35] R.-J. Cheng, P.-Y. Chen, P.-R. Gau, C.-C. Chen, S.-M. Peng, *Journal of the American Chemical Society* **1997**, *119*, 2563-2569.

[36] W. R. Scheidt, C. A. Reed, *Chemical reviews* **1981**, *81*, 543-555.

[37] M. Atanasov, P. Surawatanawong, K. Wieghardt, F. Neese, *Coord. Chem. Rev.* **2013**, *257*, 27-41.

[38] A. D. Becke, *The Journal of Chemical Physics* **1993**, *98*, 1372-1377.

[39] D. Sellmann, T. Hofmann, F. Knoch, *Inorg. Chim. Acta* **1994**, *224*, 61-71.
[40] D. Sellmann, W. Soglowek, F. Knoch, G. Ritter, J. Dengler, *Inorganic Chemistry* **1992**, *31*, 3711-3717.
[41] K. P. Jensen, J. Cirera, *J. Phys. Chem. A* **2009**, *113*, 10033-10039.
[42] M. Reiher, *Inorganic Chemistry* **2002**, *41*, 6928-6935.
[43] R. K. Szilagyi, M. A. Winslow, *Journal of Computational Chemistry* **2006**, *27*, 1385-1397.
[44] J. P. Perdew, *Physical Review B* **1986**, *33*, 8822-8824.
[45] G. D. Fallon, B. M. Gatehouse, P. J. Marini, K. S. Murray, B. O. West, *J. Chem. Soc.-Dalton Trans.* **1984**, 2733-2739.
[46] K. Ray, E. Bill, T. Weyhermuller, K. Wieghardt, *Journal of the American Chemical Society* **2005**, *127*, 5641-5654.
[47] J. N. Harvey, M. Aschi, *Faraday Discuss.* **2003**, *124*, 129-143.
[48] R. L. Martin, A. H. White, *Inorganic Chemistry* **1967**, *6*, 712-&.
[49] M. E. Ali, *J. Phys. Chem. B* **2012**, *116*, 5849-5859.
[50] D. H. Dolphin, J. R. Sams, T. B. Tsin, *Inorganic Chemistry* **1977**, *16*, 711-713.
[51] A. L. Balch, *Inorganic Chemistry* **1971**, *10*, 276-281.
[52] M. A. Halcrow, *Polyhedron* **2007**, *26*, 3523-3576.
[53] H. Paulsen, V. Schunemann, J. A. Wolny, *European Journal of Inorganic Chemistry* **2013**, 628-641.
[54] M. Sorai, S. Seki, *J. Phys. Chem. Solids* **1974**, *35*, 555-570.
[55] G. Brehm, M. Reiher, S. Schneider, *J. Phys. Chem. A* **2002**, *106*, 12024-12034.
[56] M. Swart, *J. Chem. Theory Comput.* **2008**, *4*, 2057-2066.
[57] M. Swart, A. W. Ehlers, K. Lammertsma, *Molecular Physics* **2004**, *102*, 2467-2474.
[58] E. Konig, K. Madeja, *Chem. Commun.* **1966**, 61-62.
[59] S. Rackwitz, W. Klopper, V. Schünemann, J. A. Wolny, *Physical chemistry chemical physics : PCCP* **2013**, *15*, 15450-15458.
[60] K. P. Kepp, *J. Inorg. Biochem.* **2011**, *105*, 1286-1292.
[61] S. Mossin, B. L. Tran, D. Adhikari, M. Pink, F. W. Heinemann, J. Sutter, R. K. Szilagyi, K. Meyer, D. J. Mindiola, *Journal of the American Chemical Society* **2012**, *134*, 13651-13661.
[62] M. Piacenza, I. Hyla-Kryspin, S. Grimme, *Journal of Computational Chemistry* **2007**, *28*, 2275-2285.
[63] R. Ahlrichs, M. Bär, M. Häser, H. Horn, C. Kölmel, *Chemical Physics Letters* **1989**, *162*, 165-169.
[64] A. D. Becke, *Physical Review A* **1988**, *38*, 3098-3100.
[65] S. H. Vosko, L. Wilk, M. Nusair, *Can. J. Phys.* **1980**, *58*, 1200-1211.
[66] P. Stephens, F. Devlin, C. Chabalowski, M. J. Frisch, *The Journal of Physical Chemistry* **1994**, *98*, 11623-11627.
[67] C. Lee, W. Yang, R. G. Parr, *Physical Review B* **1988**, *37*, 785-789.
[68] J. M. Tao, J. P. Perdew, V. N. Staroverov, G. E. Scuseria, *Physical Review Letters* **2003**, *91*.
[69] O. Treutler, R. Ahlrichs, *The Journal of Chemical Physics* **1995**, *102*, 346-354.
[70] A. Schäfer, C. Huber, R. Ahlrichs, *The Journal of Chemical Physics* **1994**, *100*, 5829-5835.
[71] S. Grimme, J. Antony, S. Ehrlich, H. Krieg, *The Journal of Chemical Physics* **2010**, *132*, 154104-154101-154104-154119.
[72] A. Schaefer, A. Klamt, D. Sattel, J. Lohrenz, F. Eckert, *Physical chemistry chemical physics : PCCP* **2000**, *2*, 2187-2193.
[73] D. A. McQuarrie, J. D. Simon, *Physical Chemistry: A Molecular Approach*, University Science Books, **1997**.
[74] A. E. Reed, R. B. Weinstock, F. Weinhold, *The Journal of Chemical Physics* **1985**, *83*, 735-746.

Received: ((will be filled in by the editorial staff))
Published online: ((will be filled in by the editorial staff))

## Entry for the Table of Contents

## Layout 1:

---

**Key Topic**

Text for Table of Contents – max. 350 characters; not the same text as the Abstract.

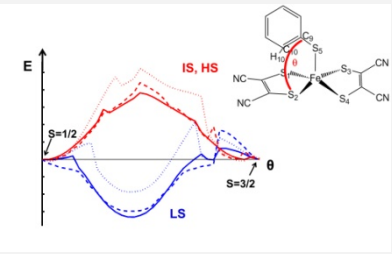


**Eileen Edler and Matthias Stein***

Page No. – Page No.

Spin-State Dependent Properties of an Iron(III) Hydrogenase Mimic

**Keywords:** mononuclear Fe(III) / proton reduction / spin transition / hydrogenases